Fuel 393 (2025) 134977

Contents lists available at ScienceDirect

Fuel

journal homepage: www.elsevier.com/locate/fuel

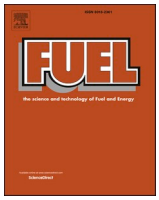

Full Length Article

Material characterization and engineering performance evaluation of phosphogypsum as a high-performance filler for bituminous pavements

Xiong Xu [a,b,c], Guohao Xu [a,b], Xiaomei Huang [a,b], GM Badiul Alam [d], Xuyong Chen [a,b,**], Anand Sreeram [e,*]

[a] School of Civil Engineering and Architecture, Wuhan Institute of Technology, Wuhan, China
[b] Hubei Provincial Engineering Research Center for Green Civil Engineering Materials and Structures, Wuhan Institute of Technology, Wuhan, China
[c] Engineering Research Center of Phosphorus Resources Development and Utilization of Ministry of Education, Wuhan Institute of Technology, Wuhan, China
[d] School of International Education, Wuhan Institute of Technology, Wuhan, China
[e] Nottingham Transportation Engineering Centre (NTEC), University of Nottingham, Nottingham, United Kingdom

ARTICLE INFO

Keywords:
Phosphogypsum
Alternative fillers
Polymeric diphenylmethane diisocyanate
Asphalt mixture
Moisture-induced damage
Performance evaluation
Mechanism analysis

ABSTRACT

The effective recycling of waste materials as alternatives to traditional mineral fillers in asphalt mixtures has both economic and environmental benefits. Phosphogypsum (PG), as one of the industrial solid wastes is a promising alternative to be used in asphalt mixture. However, in terms of the physical nature of PG, its high-absorption and moisture-expansion cause significant deterioration in engineering properties, particularly moisture-induced damage. To address these concerns, this study considered adopting polymeric diphenylmethane diisocyanate (PMDI) to activate asphalt binder with the introduction of active isocyanate (–NCO) groups, to chemically capture and stabilize the treated PG (TPG) fillers in the mixture. Based on this, the moisture-induced properties and other engineering performances of TPG-containing asphalt mixture (PGAM) with various PMDI contents were evaluated through a series of mechanical tests, and the chemical interaction mechanism between PG and PMDI in asphalt mixture was further simulated and analysed by X-ray diffraction (XRD), infrared spectroscopy (FTIR), thermogravimetry–differential thermogravimetry (TG-DTG), X-ray photoelectron spectroscopy (XPS), and scanning electron microscopy (SEM) tests. The results indicated that PMDI can effectively improve the moisture-induced performance of PGAM, in addition to enhancing the high- and low-temperature stability and reducing rutting and cracking risks. The thermal and microstructural analyses confirmed PMDI in asphalt binder helps consume water released from TPG fillers through promoting the formation of surface coatings, while also enhancing chemical bonding with –OH groups on mineral aggregates. Overall, the recycling approach developed in this study provides an effective solution for improving the engineering performance of PG in asphalt pavement applications.

1. Introduction

Asphalt pavements are the most common type of road pavements worldwide, and offers superior driving comfort, convenient construction, and adaptability in comparison with concrete pavements [1–3]. Asphalt mixtures are a viscoelastic composite material formed by asphalt, aggregates, and fillers in specific proportion [4,5]. The bonding behavior of coarse aggregates in mixture comes from asphalt mastic composed of asphalt binder and fine aggregates including mineral fillers, which has significant impacts on the mixture performance [6,7]. Hence, mineral filler is one of the most important components contributing to the overall quality of asphalt pavements.

Along with the increasing construction of asphalt pavements, the demand for mineral fillers are also increasing in practical applications [8,9]. Mineral fillers are being continuously consumed to cause the reduction or shortage of natural resources, which have led to the increase in construction expense and resulting ecological ramifications [10]. Therefore, it is necessary and valuable to seek low-cost alternatives

* Corresponding author at: Nottingham Transportation Engineering Centre (NTEC), Faculty of Engineering, University of Nottingham, Nottingham NG7 2RD, UK. (Anand Sreeram).
** Corresponding author at: School of Civil Engineering and Architecture, Wuhan Institute of Technology, Wuhan, China (Xuyong Chen).
E-mail address: anand.sreeram@nottingham.ac.uk (A. Sreeram).

https://doi.org/10.1016/j.fuel.2025.134977
Received 17 December 2024; Received in revised form 13 January 2025; Accepted 3 March 2025
Available online 9 March 2025

Table 1
Physical properties of asphalt binder.

Item	Test result	Requirement	Standard
Softening point (°C)	48.2	≥46	ASTM D36
Ductility at 15°C (cm)	>100	100	ASTM D113
Penetration at 25 °C (0.1 mm)	69	60–80	ASTM D5
Viscosity at 135°C (Pa·s)	0.45	≤3	ASTM D4402

Table 2
Physical properties of PMDI.

Item	Test Result	Standard
Density at 25 °C(g·cm^{-3})	1.22	ASTM D1480
Dynamic viscosity at 25 °C (mPa·s)	200	ASTM D445
Physical state	Orange liquid	–
Flashpoint (°C)	204	ASTM D56
–NCO content	30 %	ASTM D2572-19

Table 3
Physicochemical properties of UPG and limestone mineral powder.

Filler type	Item	Test result	Standard
UPG powder	Main constitution	$CaSO_4{\cdot}2H_2O$	ASTM C471M
	Moisture content (%)	13.5	ASTM C566
	Apparent relative density	2.46	ASTM C128-15
	Average particle sizes	39.1	ASTM C110-20
	pH	5.5	ASTM C25
	Specific surface area (m^2/kg)	90	ASTM C204
Limestone mineral powder	Main constitution	$CaCO_3$	ASTM C25
	Moisture content (%)	0.5	ASTM C566
	Apparent relative density	2.71	ASTM C128-15
	Average particle sizes	18.6	ASTM C110-20
	pH	8.9	ASTM C25
	Specific surface area (m^2/kg)	410	ASTM C204

to replace natural mineral fillers for sustainable construction of asphalt pavement.

Solid wastes may be a cost-effective option as they are grinded into powders at a filler scale [11]. During the past decades, fillers have been generated at a large scale due to the rapid development of industry, agriculture, and urban areas, including PG, fly ash, waste concrete [12,13]. If these wastes can be properly handled or disposed of, the negative impacts on the ecological environment and public health can be mostly avoided [14,15]. Current studies have shown that solid wastes can be effectively used as alternatives for mineral fillers to prepare asphalt mixtures [16–18]. For instance, Chen et al. [19] found the use of recycled fine aggregate powder (RFAP) as an alternative filler can enhance the moisture-induced damage resistance and fatigue resistance of asphalt mixtures. Zhang et al. [10] demonstrated that the incorporation of red mud waste as filler can benefit to improve the stiffness, elasticity, and rutting resistance to a certain extent. Chen et al. [20] discovered that steel slag powder (SSP) filler mixed in asphalt mixture shows superior resistances to permanent deformation, low-temperature cracking, and water damage, as compared to the asphalt mixture mixed with natural limestone filler.

PG, one of the industrial solid wastes, is generated from the production of phosphoric acid [21]. During the production, approximately 4.5−5 tons of PG will be produced for one ton of phosphoric acid [22]. PG is mainly composed of calcium sulfate dihydrate ($CaSO_4{\cdot}2H_2O$), which is limited to be widely used in practical engineering due to its susceptibility to moisture and harmful elements [23,24]. The indiscriminate discharge and accumulation of PG can squander land resources, contaminate groundwater resources, as well as severely degrade the ecological environment [25,26]. These factors obviously increases difficulties in adopting PG as filler in asphalt pavement if no further measures are considered.

As of now, there have a few studies published in regard to how to properly recycle PG as a modifier or filler in asphalt mixtures. For instance, Cuadri et al. [27] used sulfuric acid to treat PG as a bituminous modifier, and found that the temperature sensitivity and rheological properties of asphalt binder can be significantly improved by adding 10 wt% treated PG at elevated temperatures. Amrani et al. [28] compared the differences of PG, fly ash, and dry phosphorus mud as fillers in asphalt mortar and discovered that PG has more significant merits in contributions to mechanical properties and rutting resistance of asphalt mortar in contrast to fly ash and phosphorus mud. Metha et al. [29] combined PG and cement as fillers instead of conventional mineral powders, and found that the suggested fillers have capacity of improving the engineering properties of asphalt mixture, including Marshall stability. These studies demonstrated that PG can be applied in asphalt pavement for some potential performance benefits if it can be well treated. However, almost all studies have focused on the engineering performance of asphalt mixtures containing PG filler (PGAM), whereas important investigation on water stability improvement method and mechanism analysis of PGAM are still not yet understood.

To fill this research gap, this study proposes to use polymerized diphenylmethane diisocyanate (PMDI) to chemically activate asphalt binder with the introduction of active isocyanate (–NCO) groups for creating opportunities to capture and stabilize PG fillers in the mixture. To this end, the moisture-induced properties and other engineering performances of PGAM with various PMDI contents will be evaluated through a series of mechanical tests, and the chemical interaction mechanism between PG and PMDI in asphalt mixture will be analyzed using advanced characterization tests. Overall, the work conducted in this study is theorized to provide valuable guidance for pavement designers and practitioners to build more sustainable asphalt pavements containing PG.

2. Materials and methodology

2.1. Materials

Asphalt binder. The asphalt binder used was bitumen with a Pen.70 grade, supplied by a local company in Wuhan City, China. The results of the physical properties are presented in Table 1.

Asphalt modifier. The polymeric diphenylmethane diisocyanate (PMDI) utilized in this study was provided by a supplier from China. It is mainly composed of 4,4′-diphenylmethane diisocyanate (MDI) and bicyclic monomer, which is an orange liquid admixture at room temperature. The main physical properties of PMDI are shown in Table 2. It is known that the active isocyanate group (–NCO) in PMDI can react with substances containing active hydrogen atoms (such as water, hydroxyl, amine, etc.) under suitable conditions, as followed by the representative reaction Equations (1), (2), and (3) [30].

Filler. The original PG powders (denoted as UPG) used in this study were provided by a factory from Yichang City in Hubei province, which were in a long-term aged state and contained less amounts of unsaturated hydroxyl from phosphate rock. Before use, the UPG powders were calcined at 160 °C for 4 h, and further adopted as alternative fillers (denoted as TPG) with a particle size less than 0.075 mm after washing and drying. To understand the differences between the UPG filler and limestone mineral filler, their main physicochemical properties are displayed in Table 3. Apart from this, the appearances of UPG, TPG, and limestone mineral fillers are shown in Fig. 1.

Aggregate. The limestone aggregates were provided by a local supplier at Wuhan city, China. This study used those more than 2.36 mm as coarse aggregates and 0.075−2.36 mm as fine aggregates. After

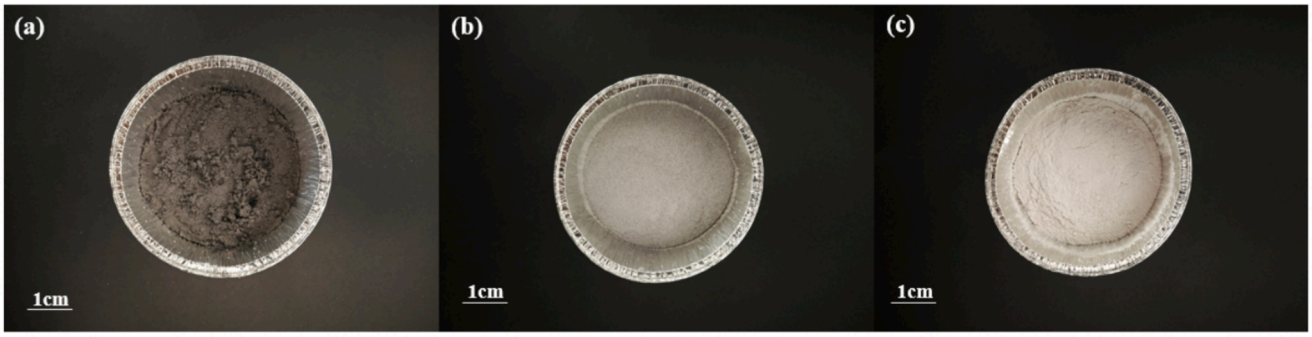

Fig. 1. Appearances of (a) UPG, (b) TPG, and (c) limestone mineral powder.

Table 4
Physical properties of aggregate.

Aggregate type	Item	Test Result	Requirement	Standard
Coarse aggregate (>2.36 mm)	Apparent relative density	2.864	≥2.60	ASTM C29
	Water absorption (%)	1.71	≤2.0	ASTM C127-15
	Crushing value (%)	16.2	≤26	ASTM C131
	Firmness coefficient (%)	3.2	≤12	ASTM D2938-95
Fine aggregate (0.075 ~ 2.36 mm)	Apparent relative density	2.749	≥2.50	ASTM C128-15
	Firmness coefficient (> 0.3 mm)	3.2	≤12	ASTM D2938-95
	Firmness coefficient (≤0.3 mm)	2.6	≤12	ASTM D2938-95
	Sand equivalent (%)	83.3	≥60	ASTM C117

Table 5
Composition design of asphalt mixtures.

Item	Asphalt type	Filler type
Lime-AM	Virgin asphalt	Limestone
PGAM/PMDI0	Virgin asphalt	TPG
PGAM/PMDI2	2 % PMDI modified asphalt	TPG
PGAM/PMDI4	4 % PMDI modified asphalt	TPG
PGAM/PMDI6	6 % PMDI modified asphalt	TPG

Note: The content of asphalt binder, aggregate and limestone/TPG in asphalt mixtures are 4.6%, 91.6%, and 3.8%, respectively.

testing, the main physical properties of aggregate are illustrated in Table 4.

2.2. Preparation of PMDI modified asphalt binder

The PMDI modified asphalt binders were prepared following the procedures: at first, the virgin asphalt binder was heated to 160 °C until a flowing state; subsequently, PMDI was added at 2 %, 4 %, and 6 %, by weight of virgin binder, to the binder and blended at a shearing speed of 4000 rpm for 30 min, respectively; and finally, the modified asphalt binders were collected for mixture fabrication. For brief expressions, these modified asphalt binders are orderly denoted as PMDI2, PMDI4, and PMDI6, respectively, and as for virgin binder, it is denoted as PMDI0 (see Table 5).

2.3. Mix design and sample preparation of PGAM

Asphalt concrete with a 13 mm-nominal maximum aggregate size (AC-13) is a commonly-used aggregate gradation for surface-paving construction of highways and expressways in China [31]. One of the AC-13 aggregate gradations was selected for this study and depicted in Fig. 2. In terms of the preparation of target asphalt mixtures for different testing programs, all the asphalt binder content was the same, controlled at 4.8 % and air void ranging from 3 % to 6 % (see Table 6.).

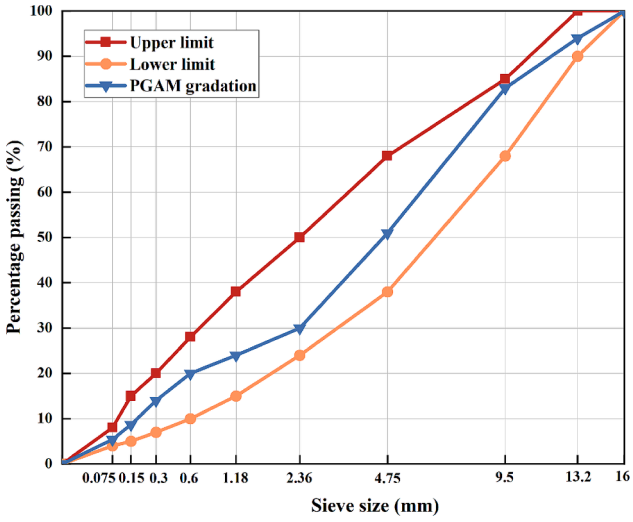

Fig. 2. Design gradation curve of asphalt mixture.

Table 6
Fabricating and testing programs of asphalt mixtures.

Property	Fabricating method	Sample dimension	Test method	Test standard
Moisture-induced stability after immersion	Marshall compaction	φ101.6 mm × 63.5 mm	Marshall test	ASTM D6927-15
Moisture-induced stability after freeze–thaw	Marshall compaction	φ101.6 mm × 63.5 mm	Indirect tensile strength test	ASTM D6931-17
Marshall stability after wet-curing	Marshall compaction	φ101.6 mm × 63.5 mm	Marshall test	ASTM D6927-15
High-temperature stability	Rolling	300 mm × 300 mm × 50 mm	Wheel tracking test	AASHTO TP63-09
Low-temperature stability	Marshall compaction	φ101.6 mm × 63.5 mm	Indirect tensile strength test	ASTM D6931-17

2.4. Marshall stability (MS) test

The immersed Marshall stability was used to assess the stripping resistance of PGAM containing various contents of PMDI while being

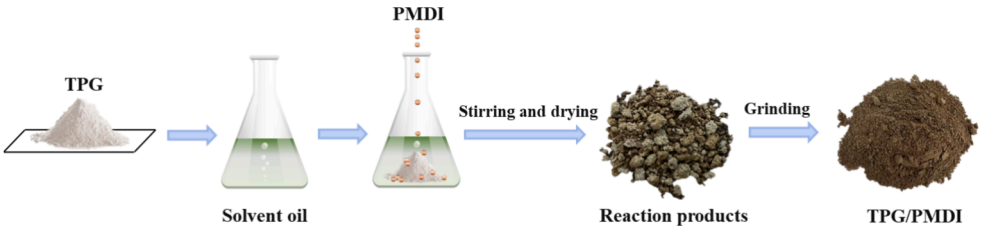

Fig. 3. Mixing and postprocessing procedures of TPG and PMDI.

Table 7
Pretreatment method design for PG.

Item	Pretreatment method	Mixing proportion	
		UPG or TPG	PMDI
UPG	Untreated, wash, and dry	/	/
TPG	Calcinate, wash, and dry	/	/
TPG/PMDI0.1	Calcinate, wash, mix, dry, and grind	1	0.1
TPG/PMDI0.2	Calcinate wash, mix, dry, and grind	1	0.2

Note: PMDI0.1 and PMDI0.2 refer to that the incorporating percentage of PMDI accounts for 10% and 20%, respectively, by weight of UPG or TPG.

exposed to water for hours. According to ASTM D6927-15, the Marshall specimens were first immersed in a 60 °C-water bath for 30 min and 48 h, respectively, and then they were separately subjected to the loading at a rate of 50 mm/min ± 5 mm/min for acquiring the Marshall load. After this, the immersed Marshall stability, namely the residual Marshall stability (RMS), can be calculated following the Equation (4).

To further understand how the moisture-induced performance of PGAM benefits from the changing content of PMDI, the Marshall stabilities of specimens after wet-curing conditions with time were comparatively evaluated in this study. The experimental setups were as follows: the specimens were first placed in a 25°C incubator with a 95 % humidity for curing for 0 h, 12 h, 24 h, 36 h, and 48 h, respectively; and once the curing time was reached, the Marshall stability test was then conducted after the specimens went through a 60°C immersion for 30 min.

2.5. Indirect tensile strength (ITS) test

The ITS test was employed in this study to understand how the tensile strength development of PGAM after being subjected to freeze–thaw condition. According to ASTM D4867, Prior to test, the specimens first underwent vacuum and pre-wetting treatments and then get conditioned at −18 ± 3°C for 16 h and 60 ± 1°C for 24 h in freeze–thaw device. Finally, the preconditioned and unconditioned specimens were moved into a 25°C-water bath for 2 h for ITS test.

According to ASTM D6931-17, the ITS test was conducted with a loading rate of 50 mm/min to determine the tensile strength of target specimens before and after one freeze–thaw cycle. Based on this, the indirect Tensile Strength Ratio (TSR) can be calculated following the Equation (5).

2.6. Wheel tracking test (WTT)

WTT was used in this study to evaluate the effect of PMDI on the rutting resistance of PGAM under repeated wheel loads at higher temperature. According to AASHTO TP63-09, the target mixture slabs with dimensions of 300 mm × 300 mm × 50 mm were fabricated for one-day stay, and subsequently, they were placed into a 60°C-chamber for 5 h. After this, the specimens were tested one by one under an applied wheel load of 0.7 MPa with a round-trip rolling speed of 42 passes for 60 min. On this basis, the rut depth for each was recorded and its development was derived by calculations for high-temperature evaluations. Herein, the specimens for the same mixing proportions were repeated three times to ensure the data accuracy.

2.7. Low-temperature performance test

The long-temperature performance was characterized in this study to demonstrate the cracking behavior of target PGAM mixtures through the comparative evaluations from Indirect Tensile (IDT) test conducted by universal testing machine (UTM-100). According to ASTM D6931, the IDT test was performed at a temperature of −10°C ± 0.5°C with a constant loading rate of 1 mm/min, while the load-deformation curve was recorded until failure. After test, the indirect tensile strength (R_T), Poisson's ratio (μ), failure tensile strain (ε_T), and failure stiffness modulus (S_T) were calculated by the Equations (6) ~ (9).

Other than the abovementioned, the stress–strain curve can also be interpreted by the load-deformation data results [32,33]. On this basis, the fracture energy (*FE*), for characterizing the withstanding of specimen from tensile load and crack expansion, can be calculated by the Equation (10) [34].

2.8. Test methods for chemical mechanism analysis

To further reveal the chemical reaction mechanism between PMDI and TPG in asphalt mixtures, this study proposed to use solvent oil that can be easily volatilized at lower temperatures to replace asphalt binder, providing a simple mixing environment for both. After mixing, the mixtures were first sent for drying at approximately 50 °C for hours to completely remove the solvent oil and then slightly grinded for powder formation, as displayed in Fig. 3. Comparatively, the pretreatment methods designed for chemical mechanism analysis are presented in Table 7. Furthermore, a series of characterizing tests including X-ray diffraction (XRD), thermogravimetry–differential thermogravimetry (TG-DTG), Fourier transform infrared spectroscopy (FTIR), X-ray photoelectron spectroscopy (XPS), and scanning electron microscopy (SEM) were conducted for chemical interaction mechanism analysis, which are briefly introduced in the following subsections.

(1) XRD test

The XRD test was used in this study to analyze the change of crystalline structure of TPG after pretreatments for understanding how PMDI works in solvent oil or asphalt binder to chemically capture the TPG particles. During the test, the Ultima IV X-ray diffractometer was utilized to radiate the test samples with an employment of Cu-target Kα line at a wavelength of 1.5406 Å. After examining, the XRD pattens were recorded for chemical analysis.

(2) TG-DTG test

The TG-DTG test was adopted in this study to acquire the thermal information of target samples, including mass loss, phase changes, and chemical composition, within a ranging control of temperature. During the test, the PerkinElmer STA 8000 TG apparatus was employed to check the thermal properties for all selected samples in nitrogen atmosphere at a heating growth rate of 20°C·min^{-1} within the temperature range

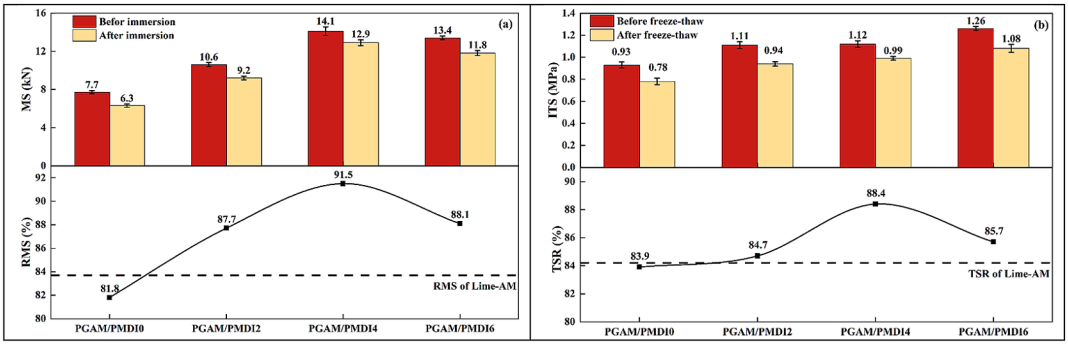

Fig. 4. Effect of PMDI contents on the moisture-induced performance of PGAM:(a) Immersed MS and (b) Freeze-thawed ITS.

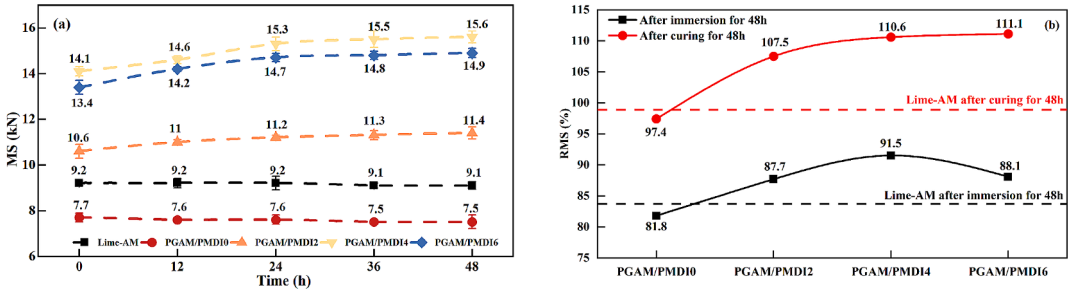

Fig. 5. Effect of wet-curing on the moisture-induced performance of PGAM/PMDI: (a) MS and (b) RMS.

between 30°C and 600°C. Afterwards, the TG-DTG profiles were collected for the key information outputs, to analyze whether PDMI can be chemically coated on the surface of TPG particles for good thermal stability while being applied in practice.

(3) FTIR test

The FTIR test was utilized in this study to understand if the PMDI can be chemically adhered to the surface of TPG particles by detecting the changes in molecular structure. For this purpose, a Nicolet Nexus 470 FTIR spectrometer was employed to identify the changes in characteristic groups of spectral brands at molecular level. The main test setups were as follows: wavenumber range of 4000–400 cm^{-1}, 32 of scanning times, and resolution of 4 cm^{-1}.

(4) XPS test

The XPS test was used in this study to analyze the surface chemical state, including the element distribution and composition, of TPG particles treated by PMDI. Based on this, it could be strongly support in terms of chemical evidence the interactions between TPG and PMDI, providing further insights into their mutual reaction mechanism from semi-quantitative resultant analyses of newly-merged and disappeared chemical structures. Prior to the test, the powdery samples were treated to remove the impurities following the as-common surface cleaning and drying procedures. After this, the samples were tested using a Mono Al Kα source at working voltage of 12 kV and filament current of 6 mA with a spot size of 400 μm by a Thermo Scientific K-Alpha XPS instrument. For full and narrow spectral scanning, the energies were 150 eV and 50 eV, with a step size of 1 eV and 0.1 eV, respectively. With the results, the data were processed to the outputs of full spectra and fitted to high-resolution spectra of C1s and N1s using an Advantage software, for overall analyses of elements and chemical states.

(5) SEM test

The SEM test was employed in this study to comparatively evaluate the influence of PMDI content on the surface state of TPG particles in microstructural morphology. Before the test, the target samples were first affixed to the sample holders with conductive adhesive and then gold-sputtered and vacuum-processed. Afterwards, they were placed in the test chamber for testing. As for this, a Zeiss Gemini 300 SEM apparatus was adopted to capture the morphological images of samples at magnification of 5,000 with appropriate controls of conditions including voltage.

3. Results and discussion

3.1. Moisture-induced performance evaluation

(1) Immersed MS and freeze-thawed ITS analysis

Fig. 4 displays the effect of PMDI contents on the moisture-induced performance of PGAM. As illustrated in Fig. 4(a), with the increasing content of PMDI, the MS value presents a first-increase-and-then-decrease trend regardless of immersion, which reaches the peak load at 14.1kN before immersion and remains the peak load at 12.9kN after immersion, respectively, as the PMDI content is 4 %. Correspondingly, the RMS value shows the same development as the PMDI content increases, which reaches the peak at 91.5 % while using 4 % PMDI. In addition, it is worthwhile noting that as compared to the PG-free mixture, PGAM/PMDI0 has a lower RMS value at 81.8 % whereas the others containing 2 %, 4 %, and 6 % PMDI have increasingly higher RMS value at 87.7 %, 91.5 %, and 88.1 %, respectively.

Similarly, from Fig. 4(b), it is clear that with the increasing PMDI content from 2 % to 6 %, the ITS values of PGAM increase slightly irrespective of freeze–thaw, but correspondingly, the TSR value first increases and then decreases with the peak at 88.4 %. These results obtained indicated that the total use of TPG, instead of limestone mineral powder, causes a moisture-induced performance deterioration of asphalt mixture no matter immersion or freeze–thaw, while PMDI can positively overcome this problem for significant performance

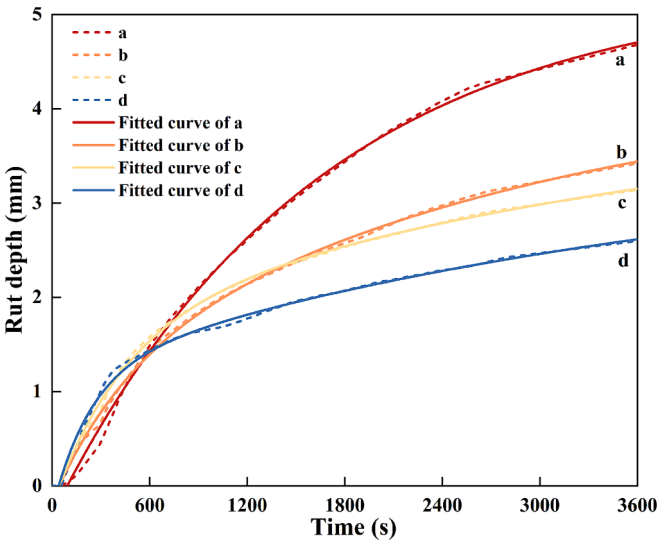

Fig. 6. Effect of PMDI contents on rut depth of PGAM at 60 °C: (a) PGAM/PMDI0, (b) PGAM/PMDI, (c) PGAM/PMDI4, and (d) PGAM/PMDI6.

Table 8
Fitted equation extracted for the variation prediction in rut depth.

Item	Fitted equation	R_1^2
PGAM/PMDI0	y = -2.83*exp(−x/1620.61)-2.79exp(−x/1620.66) + 5.32	0.998
PGAM/PMDI2	y = -1.33*exp(−x/464.07)-3.24exp(−x/2984.37) + 4.41	0.999
PGAM/PMDI4	y = -1.89*exp(−x/447.82)-2.56*exp(−x/4288.45) + 4.26	0.999
PGAM/PMDI6	y = -1.45*exp(−x/233.82)-2.33*exp(−x/3846.73) + 3.53	0.996

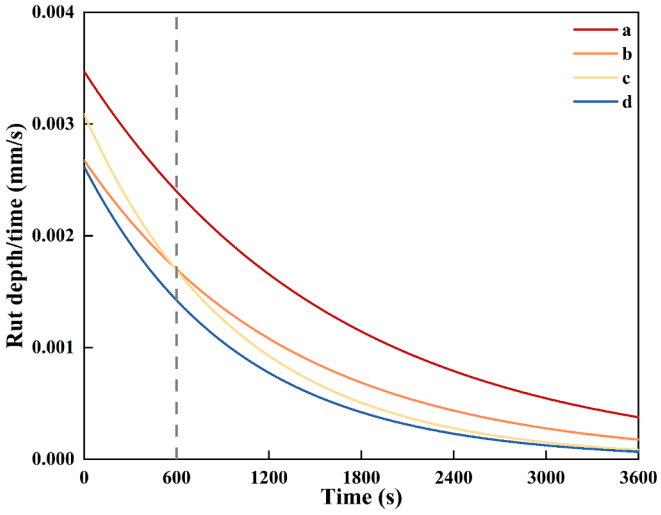

Fig. 7. Effect of PMDI contents on rut depth developing rate of PGAM at 60 °C: (a) PGAM/PMDI0, (b) PGAM/PMDI, (c) PGAM/PMDI4, and (d) PGAM/PMDI6.

improvements, particularly its use at 4 %, by weight of virgin bitumen [35].

(2) Cured MS analysis

Fig. 5 reflects the effect of wet-curing on the moisture-induced performance of PGAM/PMDI. From Fig. 5(a), it is clear that with the elapse

Table 9
Differential fitting equation and the critical index on the rut depth change rate.

Item	Differential fitted equation	R_2^2
PGAM/PMDI0	$y_1 = 3.47*10^{-3}*\exp(-x/1621.25)-4.98*10^{-7}$	0.997
PGAM/PMD2	$y_1 = 2.68*10^{-3}*\exp(-x/1322.46)-8.32*10^{-8}$	0.996
PGAM/PMDI4	$y_1 = 3.09*10^{-3}*\exp(-x/996.32)-1.02*10^{-7}$	0.998
PGAM/PMDI6	$y_1 = 2.62*10^{-3}*\exp(-x/984.68)-1.84*10^{-7}$	0.998

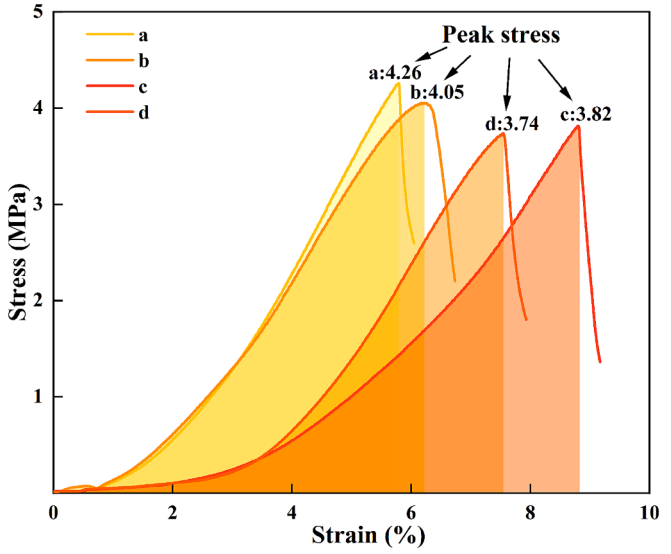

Fig. 8. Stress–strain curve and fracture energy of PGAM/PMDI at −10 °C: (a) PGAM/PMDI0, (b) PGAM/PMDI, (c) PGAM/PMDI4, and (d) PGAM/PMDI6.

Table 10
Low-temperature performance test results.

Item	Fracture energy (J·m^{-2})	Damaged tensile strain (%)	Damaged stiffness modulus (MPa)
PGAM/PMDI0	892	5.7	1264.8
PGAM/PMDI2	1028	6.2	1130.1
PGAM/PMDI4	998	8.8	884.9
PGAM/PMDI6	836	7.5	852.9

of wet-curing time the MS values of PGAM/PMDI somewhat increase irrespective of PMDI content, which of Lime-AM and PGAM/PMDI0 show no significant changes. In addition, it is also observed that compared to Lime-AM, PGAM/PMDI0 has lower MS values of 7.7kN at 0 h and 7.5kN at 48 h, but PGAM/PMDI2, PGAM/PMDI4, and PGAM/PMDI6 have higher MS values of 10.6kN, 14.1kN, and 13.4kN at 0 h and 11.4kN, 15.6kN, and 14.9kN at 48 h, respectively. These results indicated that PMDI can not only compensate the mixture stability loss caused by the filler replacement from limestone to TPG but also significantly increase the mixture stability of PGAM, which however will not lastingly contribute to the mixture stability enhancement with an excessive content. The reason can be that appropriate amounts of –NCO groups from PMDI in asphalt binder chemically interact with the released water from TPG and –OH groups from aggregate surface for freshly mixed PGAM, and residual amounts of –NCO groups continue interacting with the water from humid environments during the service time [36].

Fig. 5(b) displays the RMS changes after immersion and curing for 48 h. It is obvious that with the increasing content of PMDI from 0 % to 6 %, the RMS value of PGMA first increases fast and then become stable

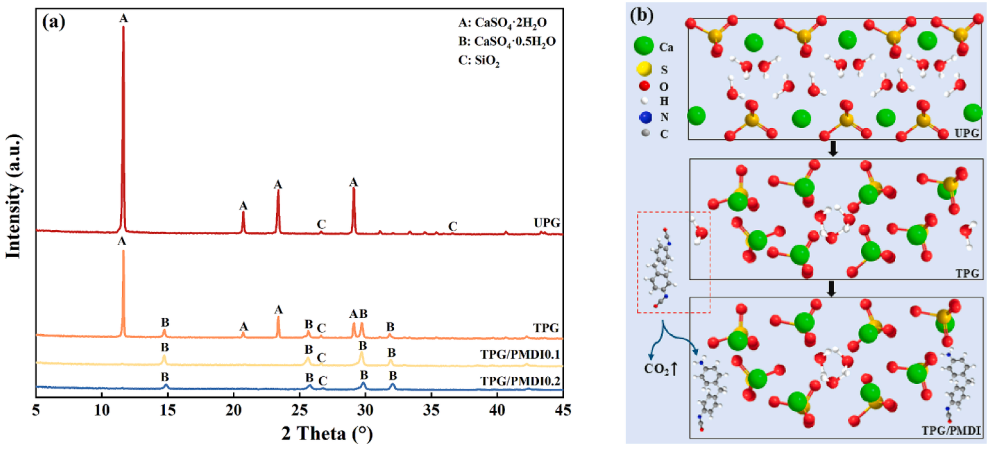

Fig. 9. The XRD test results (a) and the crystal structure (b) of UPG, TPG, and TPG/PMDI.

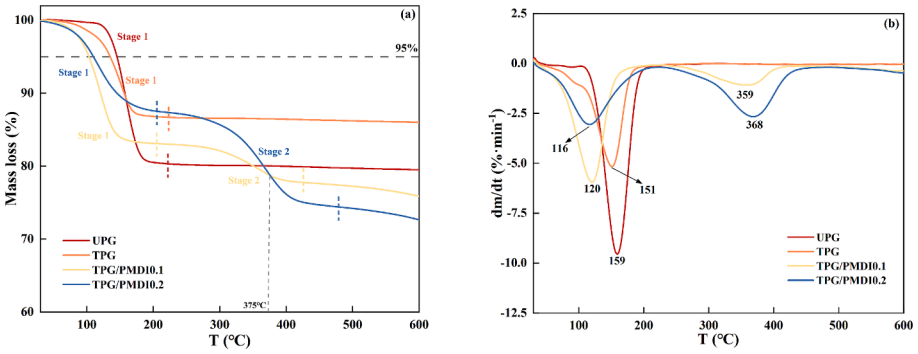

Fig. 10. Thermal analysis of UPG, TPG, and TPG/PMDI: (a) TG; and (b) DTG.

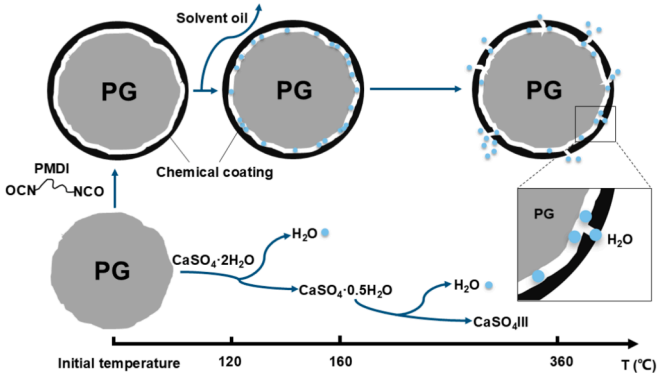

Fig. 11. PG chemical structure changes during TG process.

from 97.4 % to 111.1 % while subjected to humid environments, which first increases and then decreases with a peak value of 91.5 % at 4 % PMDI by weight of virgin binder while subjected to water immersion. The results obtained demonstrated that PMDI works effectively to enhance the mixture stability during an earlier period regardless of curing or immersion, which however at excessive content reaching 6 % causes a decreased mixture stability after immersion.

3.2. *High-temperature stability analysis*

Fig. 6 illustrates the effect of PMDI content on the rut depth of PGAM. It is evident that the rut depth of PGAM gradually decreases with the increasing content of PMDI after they are further stabilized by repeated wheel loads. Obviously, as the PMDI content is added from 0 % to 2 %, 4 %, and 6 %, the rut depth of PGAM at 3600 s decreases from 4.71 mm to 3.44 mm, 3.15 mm, and 2.61 mm, respectively. These findings showed that more incorporation of PMDI gives better resistance to PGAM deformation at elevated temperature. In addition, all rut depth developments present a good relationship with time, which have

Table 11
Thermal decomposition parameters of UPG, TPG, and TPG/PMDI.

Items	T $_{onset}$ at mass loss of 5 %·min^{-1} (°C)	Residual mass (m) at 600°C (%)	T$_{d,\ max}$ (°C)	Total component amount based on T$_{d,\ max}$	R $_{max}$	Crystal transition point (°C)
UPG	145.4	79.5	159	1	−9.54	168
TPG	135.1	86.1	151	1	−5.16	162
TPG/ PMDI0.1	109.8	75.9	120, 359	2	−5.94, −1.08	/
TPG/ PMDI0.2	103.1	72.6	116, 368	2	−3.06, −2.66	/

Note: T $_{onset}$ refers to initial decomposition temperature; T $_{d,\ max}$ refers to maximum decomposition temperature; and R $_{max}$ refers to maximum decomposition rate.

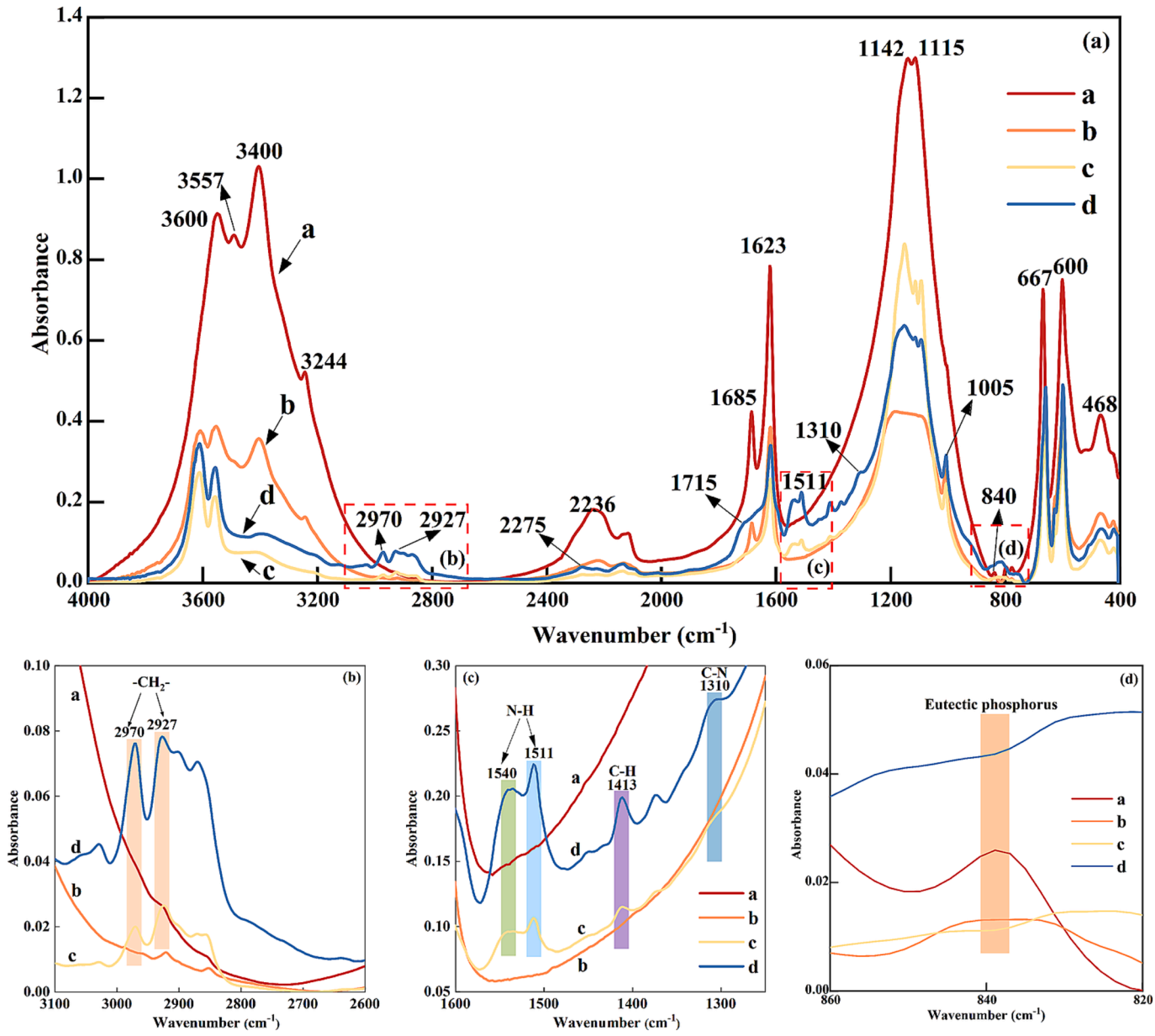

Fig. 12. (a) FTIR spectra: a. UPG, b. TPG, c. TPG/PMDI0.1, and d. TPG/PMDI0.2; (b) Absorption peak of –CH_2- stretching vibration in carboxylic acid; (c) Absorption peaks of –NH, C–H, and C-N groups; and (d) Absorption peak of eutectic phosphorus.

Table 12
Attribution of main characteristic bands of UPG, TPG, and TPG/PMDI.

Wavenumber (cm^{-1})	Vibration type
3600, 3557, 3400, 3244	H_2O stretching
2970	O–H Carboxylic acid stretching
2927	–CH_2- stretching
2275	NCO asymmetric stretching
2236	H_2O stretching
1715	C=O deformation
1685	–OH deformation
1623, 1540, 1511	–NH deformation
1413	–CH bending
1310	–CN stretching
1142, 1124, 1115, 1005	v3, v1 SO_4^{2-} asymmetrical bending
840	Eutectic phosphorus
667, 600	v4 SO_4^{2-} asymmetrical bending
468	v2 SO_4^{2-} symmetric bending

correlation coefficient (R_1^2) more than 0.996. The fitted equations extracted for the variation prediction in rut depth are displayed in Table 8, which are used to back-calculate the rut depth developing rate as presented in Fig. 6.

Fig. 7 reflects the rut depth developing rate of PGAM containing different contents of PMDI. Correspondingly, the fitted equations with correlation coefficients (R_2^2) higher than 0.996 are collected in Table 9. Compared to PGAM/PMDI0, others have lower rut depth developing rates after they are stabilized. With time towards 3600 s, they are all developed below 0.001 mm/s in rut depth rate, but significantly, PGAM/PMDI0 still has a relatively higher rut depth developing rate than others. Meanwhile, the rut depth developing rate of PGAM/PMDI2 is presented higher than that of PGAM/PMDI2 and PGAM/PMDI4. In addition, it is worthwhile noting that PGAM/PMDI4 has a slightly higher rut depth developing rate at earlier stage after 600 s and presents a closer changing rate at later stage towards 3600 s in contrast to PGAM/PMDI6. These results suggested that PMDI can reduce the rut depth developing rate of PGAM, which contributes to delaying the rutting

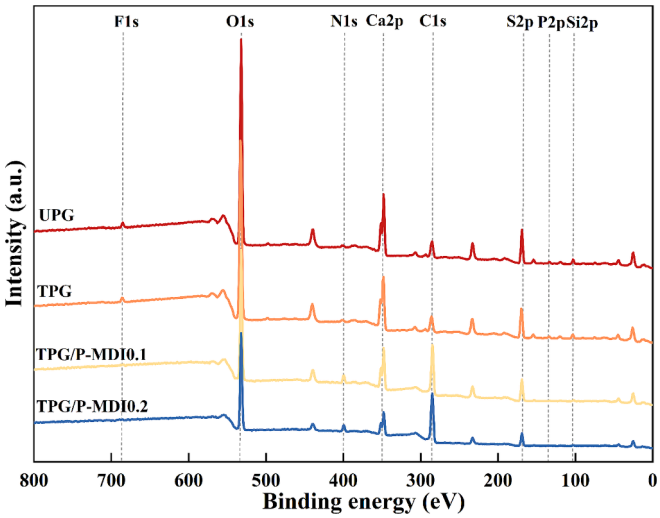

Fig. 13. Full XPS profile of UPG, TPG, and TPG/PMDI.

Table 13
Relative content of elements in UPG, TPG, and TPG/PMDI.

Items	Elemental composition (%)							
	O1s	S2p	Ca2p	C1s	Si2p	F1s	P2p	N1s
UPG	57.74	8.89	22.76	6.08	1.19	1.93	0.59	0.82
TPG	56.73	9.06	23.62	6.40	1.06	1.59	0.52	1.01
TPG/ PMDI0.1	46.45	7.85	20.30	20.41	0.52	0.85	0.35	3.27
TPG/ PMDI0.2	46.39	6.00	15.60	27.64	0.51	0.08	0.26	3.52

deformation development to large extent as it is reached at 4 %. This is because the addition of PMDI will make the modified asphalt have more complex microstructure and reduce the thermal sensitivity of the asphalt [37]. In addition, PMDI can chemically react with released water from PG, exposed –OH from aggregate surface, and free water from natural environments for structural connections, thus causing a susceptibility reduction of PGAM to high temperatures [38,39].

3.3. Low-temperature performance analysis

Fig. 8 displays the stress–strain curve and fracture energy of PGAM/PMDI at −10 °C. It is clear that as the PMDI content increases from 0 % to 2 %, 4 %, and 6 %, the peak stress of PGAM decreases from 4.26 MPa to 4.05 MPa, 3.82 MPa, and 3.74 MPa, and the corresponding strain changes from 5.7 % to 6.2 %, 8.8 %, and 7.5 %, respectively. These results indicated that PMDI will slightly produce negative impacts on the stress-induced damage of PGAM at low temperature, which however will contribute to improve the toughness to some extent. Based on this, the fracture energy, damaged tensile strain, and damaged stiffness modulus of PGAM/PMDI are calculated and presented in Table 10. As shown, the fracture energy first increases and then decreases with the increasing content of PMDI, which shows close values at 1028 J·m^{-2} and 998 J·m^{-2} for PGAM/PMDI2 and PGAM/PMDI4. In addition, damaged tensile strain slightly increases, and damaged stiffness modulus significantly decreases as the PMDI content increases. The results implied that the resistance of PGAM to cracking at low temperature can be well improved with limited amount of PMDI within 4 % by weight of virgin binder, in association with acceptable slight sacrifice of stiffness.

The reason for this is that the –NCO groups from PMDI can react with the released water from PG and the –OH from aggregates for the network structure formations to enhance the fracture toughness and fracture energy of PGAM at low temperatures. However, with an increased PMDI content, an excessive content of PMDI reacts with asphaltene components and maltene components in asphalt binder are excessively transformed into asphaltene components, which disrupts the balance between maltene and asphaltene components and results in poor compatibility [40,41]. Consequently, the low-temperature cracking resistance of the asphalt mixture is adversely affected to the decrease in the fracture energy and fracture toughness of PGAM [42,43].

3.4. XRD analysis

Fig. 9(a) indicates the XRD test results of UPG, TPG, and TPG/PMDI. Fig. 9(b) shows the crystal structure changes of them. It is evident that compared to that of UPG, the XRD patten of TPG shows four newly-merged peaks that represents calcium sulfate hemihydrate ($CaSO_4{\cdot}0.5H_2O$) and significantly diminished amounts of calcium sulfate dihydrate ($CaSO_4{\cdot}2H_2O$), while the less amount of SiO_2 is still present [44]. However, as compared to TPG, the diffraction peaks for $CaSO_4{\cdot}2H_2O$ have completely disappeared and for $CaSO_4{\cdot}0.5H_2O$ are limitedly diminished in TPG/PMDI0.1 and TPG/PMDI0.2. Especially, the peak intensity of $CaSO_4{\cdot}0.5H_2O$ in TPG/PMDI0.2 shows to be relatively lower than that in TPG/PMDI0.1. These results suggested that the calcination treatment can remove some of the crystalline water from $CaSO_4{\cdot}2H_2O$ in PG, and further, more contents of PMDI strives to chemically consume the residual $CaSO_4{\cdot}2H_2O$ and form $CaSO_4{\cdot}0.5H_2O$. The reason is that more active –NCO groups provided by PMDI can interact with less crystalline water from the mixed $CaSO_4{\cdot}2H_2O$ and $CaSO_4{\cdot}0.5H_2O$ for chemical combinations.

3.5. TG-DTG analysis

Fig. 10 displays the TG-DTG curves of UPG, TPG, and TPG/PMDI. Fig. 11 shows the PG chemical structure changes during TG process. Correspondingly, the initial decomposition temperature (T_{onset}, at 5 %

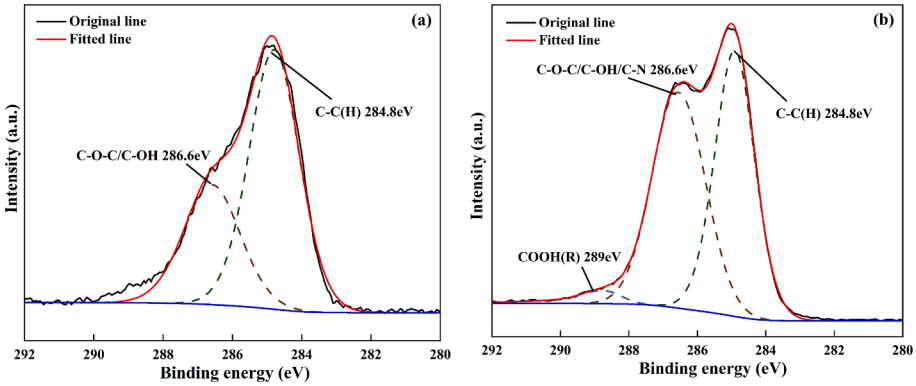

Fig.14. XPS C1s high-resolution spectrum: (a) TPG; (b) TPG/PMDI0.2.

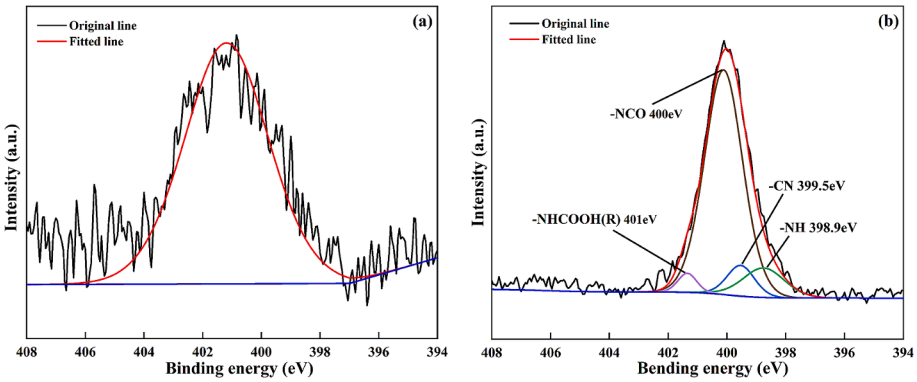

Fig. 15. XPS N1s high-resolution spectrum: (a) TPG; (b) TPG/PMDI0.2.

Table 14
Fitted results of XPS C1s and N1s high-resolution spectra of TPG and TPG/PMDI0.2.

Spectrogram	Chemical group	Relative content (%)
TPG C1s fine spectra	C–C(H) 284.8 eV	65.71
	C-O-C/C-OH 286.6 eV	34.29
TPG/PMDI0.2 C1s fine spectra	C–C(H) 284.8 eV	47.06
	C-O-C/C-OH/C-N 286.6 eV	49.88
	COOH(R) 289 eV	3.06
TPG/PMDI0.2 N1s fine spectra	–NH 398.9 eV	11.04
	–CH 399.5 eV	7.71
	–NCO 400 eV	78.01
	NHCOOH(R) 401 eV	3.24

mass loss) and the maximum decomposition rate (R_{max}) are shown in Table 11. As presented, UPG starts losing mass at around 145°C and goes to balance after 200 °C, with a R_{max} of −9.545 %·min^{-1} at 159 °C, while the total mass loss for UPG is 20.5 %. Conversely, TPG begins being dehydrated at around 135°C to thermal stabilization after approximately 200 °C with a R_{max} of −5.163 %·min^{-1} at 151 °C and a total mass loss of 13.9 %. These results indicated the selected treatment can in advance remove the crystalline water of PG by 6.6 % for the thermal stability improvement [45]. However, for TPG/PMDI0.1 and TPG/PMDI0.2, both of them present two mass loss stages in TG curves and two peaks in DTG curves, which for the first-stage represent the mass loss from the hardly removed residues of solvent oil used for simulation experiment and for the second-stage mainly refer to the mass loss of chemically formed substances coated onto the surfaces of TPG. It is worthy of noting that the maximum decompositions of crystalline water at 151−159 °C are not observed, which demonstrated that PMDI can chemically capture the released crystalline water to the newly-formed products on the surface of TPG in solvent oil, or maybe in asphalt binder, during the treatment, for reducing the risks from water attacks to the mixture.

In addition, TPG/PMDI0.2 has a total mass loss of 27.4 % and a second-stage R_{max} of −3.055 %·min^{-1} at 368°C, but by contrast, TPG/PMDI0.1 presents a total mass loss of 24.1 % and a second-stage R_{max} of −3.055 %·min^{-1} at 359°C. Before 375°C, it is clear that TPG/PMDI0.2 shows lesser mass loss during the whole thermal process as compared to TPG/PMDI0.1. These findings implied that more use of PMDI will produce a thicker protective coating onto the surface of TPG for improving the thermal stability, which significantly benefits to avoid negative impacts from water. The reason depends upon that PMDI, mixed in the medium of solvent oil or maybe asphalt binder, can chemically consume crystalline water released from TPG to produce more adhesive reaction products for providing better water-proofing protection [46]. Apart from this, it can be understood that as this asphalt mixture is applied in practice, the chemical coatings on TPG will not be damaged at maximum service temperatures such as in summer at approximately 70°C.

3.6. FTIR analysis

Fig. 12 depicts the FTIR spectra of UPG, TPG, and TPG/PMDI. Table 12 shows the attributions of main characteristic bands. It is clear that the peaks at 3600 cm^{-1}, 3554 cm^{-1}, 3400 cm^{-1}, and 3244 cm^{-1} correspond to the stretching vibrations of –OH in the crystalline water from UPG. The 1685 cm^{-1} and 1623 cm^{-1} peaks are attributed to the bending vibration absorption of –OH in the crystalline water from UPG (curve a). After pretreatment, the peak intensities at these positions significantly decrease as shown in the profile of TPG (curve b). In addition, the peak location at 1715 cm^{-1} is belonged to carbonyl (C=O) deformation vibration that related to carbamate and urea (curves c and d) [47]. The results indicated that $CaSO_4{\cdot}2H_2O$ in UPG can partially be transformed into $CaSO_4{\cdot}0.5H_2O$ after calcination. Compared to TPG, the absorption peak intensities at these positions are markedly diminished in TPG/PMDI0.1 and TPG/PMDI0.2, as well as the absorption peak of the –NH group in carbamate at 1511 cm^{-1}, which is more pronounced in TPG/PMDI0.2 (Fig. 12 (c)). These results suggested that PMDI consumes the hydroxyl groups in TPG and forms carbamate upon chemical reactions with TPG (I).

As presented in Fig. 12 (b), the absorption peaks at 2970 cm^{-1} and 2927 cm^{-1} are attributed to stretching vibrations of –OH in carboxylic acid, and the absorption peaks of C-N stretching and –NH bending vibrations are also found at 1310 cm^{-1} [42]. The stretching vibrations at 2275 cm^{-1} and at 1540 cm^{-1} are respectively attributed to the –NCO and –NH groups (Fig. 12 (c)) [48]. The results indicated that the chemical reaction between PMDI and PG produced amine salts and urea (Equation (2), (3)), and there are still unreacted free –NCO groups in TPG/PMDI0.1 and TPG/PMDI0.2. The reason is that the terminal –NCO groups at both ends of the MDI component in PMDI have latent chances to react with PG, at which some of them reacts with PG for connections and the residual groups remain opportunities to react with surrounding water for further strength enhancement in pavement service while being subjected to the natural environment [49].

3.7. XPS analysis

Fig. 13 illustrates the full XPS profile of UPG, TPG, and TPG/PMDI. The relative content of main chemical elements are presented in Table 13. As compared to UPG, TPG still has the main chemical elements including Ca, O, S, Si, C, P, and F, which showed the treatments of washing and calcination cannot remove the C based organic substances, P based insoluble substances (or called co-crystalized P), F based insoluble substances, and Si based substances in UPG. More significantly, the relative content of O decreased from 57.74 % to 56.73 %, which indicated that the treatment only causes the dehydration reaction

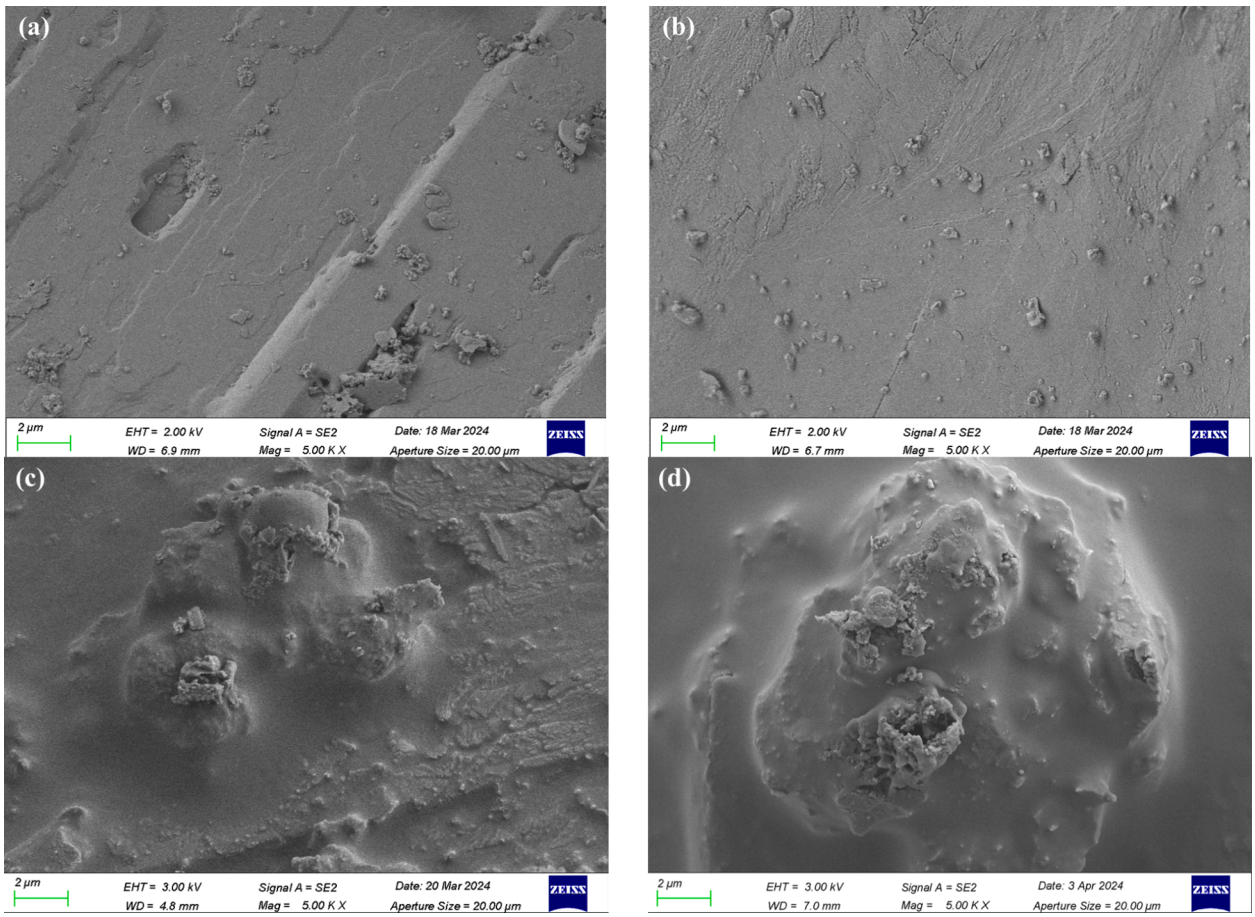

Fig. 16. Microstructural morphology: (a) UPG; (b) TPG; (c) TPG/PMDI0.1; and (d) TPG/PMDI0.2.

of crystalline water in UPG. Further, with PMDI, the weak intensity signals of F, P, and Si are all sharply decreased, even almost disappeared, in association with the decreased content of O, Ca, and S, the appearance of N, as well as the increased content of C. For O, Ca, S, N, and C, from TPG/PMDI0.1 to TPG/PMDI0.2, they change from 46.45 %, 20.30 %, 7.85 %, 3.27 %, and 20.41 %, to 46.39 %, 15.60 %, 6.00 %, 3.52 %, and 27.64 %, respectively, while for P and F they vary from 0.35 % and 0.85 % to 0.26 % and 0.08 %, respectively. These results hinted that PMDI can not only chemically interact with released crystalline water of TPG to produce surface coating materials, but also be capable of partially fixing F and P inside the surface coating materials for the reduction of pollutants.

To further understand the main molecular structure forms, the XPS C1s and N1s high-resolution spectra of TPG and TPG/PMDI0.2 are fitted as shown in Fig. 14 and Fig. 15, respectively. The relative contents of chemical structures are correspondingly presented in Table 14. From Fig. 14 and Table 14, it is obvious that the relative contents of C–C(H) and C-O-C/C-OH in TPG are 65.71 % and 34.29 %, respectively, whereas the relative contents of C–C(H), C-O-C/C-OH/C-N, and COOH(R) in TPG/PMDI0.2 are 47.06 %, 49.88 %, and 3.06 %, respectively. The results indicated that new chemical structure forms, namely C-N and COOH(R), are appeared with the introduction of PMDI to PG.

As further observed in From Fig. 15 and Table 14, there are apparently no N based functional groups on the surface of TPG. The relative contents of –NH, –CN, –NCO, and NHCOOH(R) in TPG/PMDI0.2 are 11.04 %, 7.71 %, 78.01 %, and 3.24 %, respectively. The binding energy of N1s at 398.9 eV is related to Carbamide produced in the (III) reaction. The binding energy of N1s at 399.53 eV is attributed to R-NH_2 in the (II) reaction. The N1s peak at 400 eV is attributed to the –NCO group. The binding energy of N1s at 401 eV is related to NHCOOH(R). These results of the N1s spectra show a good correspondence to those of the C1s spectra, which indicated again that PMDI can chemically react with PG in medium like solvent oil, or even in asphalt binder. The reason can be found in consistency with FTIR analysis.

3.8. SEM analysis

Fig. 16 illustrates the microstructural morphology of UPG, TPG, and TPG/PMDI with a 5, 000 × magnification. It is observed that the surface state of UPG presents to be relatively smooth, but some small defects such as micro-holes and agglomerates clearly exist, as shown in Fig. 16 (a). After calcination pretreatment, TPG still has a smooth surface with smaller particle agglomerates, as displayed in Fig. 16(b). Further, the surface becomes vague and those smaller particles are fixed under the coating of newly-formed substances with addition of PMDI, which looks more significant as the PMDI content increases, as shown in Fig. 16(c) and (d). These observations demonstrated that PMDI works effectively in medium to chemically capture TPG with the formation of organic coating materials for the reduction of moisture susceptibility. The reasons are attributed to the chemical reactions of PMDI with the released crystalline water from TPG, which are consistent with the analyses of XRD, TG-DTG, FTIR, and XPS.

3.9. Performance-enhancing mechanism analysis

Based on systematic evaluation of moisture-induced properties and other engineering performances of PGAM, in association with chemical and morphological characterizations using XRD, TG-DTG, FTIR, XPS, and SEM tests, the performance-enhancing mechanism can be characterized as shown in Fig. 17. From Fig. 17(a), it presents the chemically

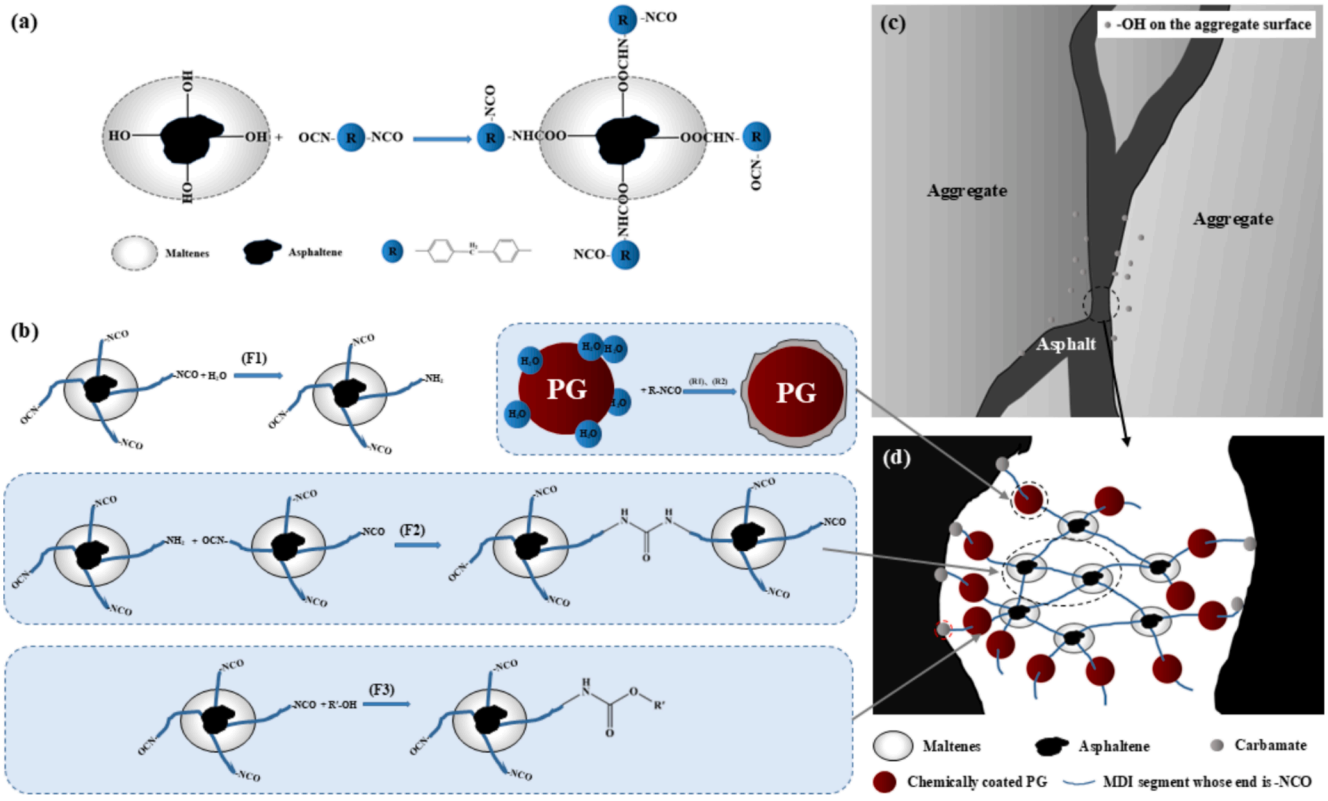

Fig. 17. The performance-enhancing mechanism of PGAM: (a) terminal –NCO groups of PMDI chemically consumes the limited –OH groups from asphaltenes in asphalt binder [41]; (b) complex chemical interactions in PGAM; (c) active asphalt binder between coarse aggregates in PGAM; and (d) full map showing the distribution state of TPG fillers in active binder between aggregates.

activating modification of asphalt binder with the addition of PMDI, which promotes the terminal –NCO groups of PMDI to chemically connect with the active oxygen-containing groups like –OH from asphaltenes in asphalt binder [50], for the partial formations of carbamate (RNHCOOR) and substituted urea ($RCO(NH_2)_2R$) [51,52]. During the modification, less amounts of –NCO groups are consumed and the residual –NCO groups make the asphalt binder active. As presented in Fig. 17(b), the active binder goes to the aggregates incorporating TPG fillers, and three parallelling chemical reactions will occur [49]. They are: (1) PMDI dynamically stabilizes TPG fillers for surface coatings through chemical reactions between –NCO and released H_2O in inner physical spaces of asphalt binder [53], as shown in Equation (1); (2) the self-reactions chemically happen between active binders, as shown in Equation (2); and (3) those –NCO groups in active binder chemically captures the –OH groups formed in the surface of natural mineral aggregates, as shown in Equation (3).

As further displayed in Fig. 17(c), the active binder can be firmly fixed onto the surface of mineral aggregates and tightly connect the coarse aggregates by chemical bonding[54]. For Fig. 17(d), it is a full map showing the distribution state of TPG fillers in active binder between aggregates, where the TPG fillers are chemically suspended with connections from crosslinking structures of active asphaltenes. Based on these chemical analyses, it is very significant that the introduction of PMDI to asphalt binder can chemically consume the released water from TPG fillers, maybe even PG fillers, for their surface coatings, and also promote the asphalt binder to be chemically active to closely adhere onto the mineral aggregates.

4. Conclusions

This study investigated adopting –NCO based PMDI as a modifier to activate virgin asphalt binder and initiate chemical interactions to capture and stabilize TPG fillers in asphalt mixtures, to address the main concern of moisture-induced damage. Through Marshall stability, indirect tensile strength test and wheel tracking test, the moisture-induced properties and other engineering performances of PGAM were systematically evaluated. The chemical interaction mechanism between TPG and PMDI in asphalt mixture was further analyzed by X-ray diffraction (XRD), Fourier transform infrared (FTIR) spectroscopy, thermogravimetry–differential thermogravimetry (TG-DTG), X-ray photoelectron spectroscopy (XPS), and Scanning electron microscopy (SEM).

The engineering performance tests show that appropriate amounts of PMDI can effectively enhance the immersed or freeze-thawed stability of PGAM and help improve the stability during an earlier period regardless of curing or immersion, but an excessive use at 6 % leads to a decreased mixture stability after immersion. PMDI contributes to decreasing the rut depth development rate of PGAM and significantly delaying the progression of rutting deformation, particularly at 4 % dosage, while the resistance of PGAM to low-temperature crack can notably be improved in association with an acceptable loss of stiffness.

The XRD and SEM tests show that new crystal structures are formed and coated onto the surface of PG after chemical interactions between PG and PMDI. The TG-DTG analysis indicated that PMDI shows capacity to capture the released crystalline water and transform it into newly formed products on the surface of TPG during treatment. FTIR and XPS tests further demonstrated the in-situ chemical reactions on the PG surface and found new C-N and COOH(R) structures formed by chemical reactions between PG and PMDI in the surface coating and fixed the F and P elements in these coating materials, thereby reducing contaminant levels. The performance-enhancing mechanism indicated that the introduction of PMDI to the asphalt binder can chemically consume the released water from TPG fillers for facilitating the formation of surface coatings, and with its chemical activation of asphalt binder.

Overall, the proposed approach opens a new avenue for recycling PG

in sustainable asphalt pavements of the future and the research conclusions can support the possible use of PGAM. However, further evaluations are required to assess the durability of PGAM, particularly its long-term resistance to water damage, aging, and fatigue. Therefore, future demonstrations of practical performance are required for engineering applications.

CRediT authorship contribution statement

Xiong Xu: Writing – review & editing, Writing – original draft, Methodology, Investigation, Funding acquisition, Formal analysis, Conceptualization. **Guohao Xu:** Writing – review & editing, Writing – original draft, Methodology, Investigation, Formal analysis. **Xiaomei Huang:** Writing – review & editing, Writing – original draft, Methodology, Investigation, Formal analysis. **GM Badiul Alam:** Writing – review & editing, Writing – original draft, Methodology, Investigation, Formal analysis. **Xuyong Chen:** Writing – review & editing, Writing – original draft, Methodology, Investigation, Formal analysis. **Anand Sreeram:** Writing – review & editing, Writing – original draft, Methodology, Investigation, Formal analysis.

Declaration of competing interest

The authors declare that they have no known competing financial interests or personal relationships that could have appeared to influence the work reported in this paper.

Acknowledgments

The authors gratefully acknowledge the support provided by the National Natural Science Foundation of China (52408287), the International Science and Technology Cooperation Projects of Hubei Province (GJHZ202400049), the Natural Science Foundation of Hubei Province (2023AFB245), and the Innovation Project of Engineering Research Center of Phosphorus Resources Development and Utilization of Ministry of Education (LCX202204).

Appendix

The reaction equations of active isocyanate group (–NCO) in PMDI react with substances containing active hydrogen atoms:

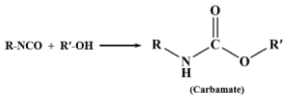

(1)

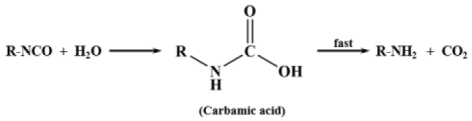

(2)

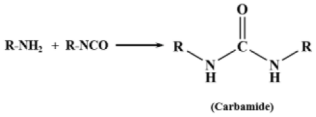

(3)

The calculation formula for the residual Marshall stability (RMS) of asphalt mixture:

$$RMS = (MS_1/MS) \times 100\% \tag{4}$$

where, MS and MS_1 refer to the Marshall load for the specimens immersed after 30 min and 48 h, respectively, kN.

The calculation formula for the indirect Tensile Strength Ratio (TSR) of asphalt mixture:

$$TSR = (ITS_1/ITS_0) \times 100\% \tag{5}$$

where, ITS_0 refers to the tensile strength of the mixture before one freeze–thaw cycle, MPa; and ITS_1 refers to the tensile strength of the mixture after one freeze–thaw cycle, MPa.

The calculation formulas of the indirect tensile strength (R_T), Poisson's ratio (μ), failure tensile strain (ε_T), and failure stiffness modulus (S_T):

$$R_T = 0.006287P_T/h \tag{6}$$

$$\mu = (0.1350A - 1.7940)/(-0.5A - 0.0314) \tag{7}$$

$$\varepsilon_T = X_T \times (0.0307 + 0.0936\mu)/(1.35 + 5\mu) \tag{8}$$

$$S_T = P_T \times (0.27 + 1.0\mu)/(h \times X_T) \tag{9}$$

where, P_T refers to the maximum value of test load, N; h refers to the height of the specimen, mm; A refers to the vertical-to-horizontal ratio in deformation of the specimen after failure, namely $A = Y_T/X_T$; and Y_T and X_T refer to the total vertical and horizontal deformations of the specimen, respectively, as reached at the maximum destructive load, mm.

The calculation formula of the fracture energy (FE) of specimen:

$$FE = \int_0^{\varepsilon_f} S(\varepsilon)d\varepsilon \tag{10}$$

where, ε_f is the strain at the maximum fracture stress, %.

Data availability

Data will be made available on request.

References

[1] Wang F, Hoff I, Yang F, Wu S, Xie J, Li N, et al. Comparative assessments for environmental impacts from three advanced asphalt pavement construction cases. J Clean Prod 2021;297:126659.
[2] Xu X, Sreeram A, Leng Z, Yu J, Li R, Peng C. Challenges and opportunities in the high-quality rejuvenation of unmodified and SBS modified asphalt mixtures: State of the art. J Clean Prod 2022;378:134634.
[3] Yan C, Xi J, Ai C, Leng Z. Investigating the unique entropy-elasticity of polymer modified asphalt. Cleaner Mater 2024;11:100216.
[4] Wu W, Jiang W, Yuan D, Lu R, Shan J, Xiao J, et al. A review of asphalt-filler interaction: mechanisms, evaluation methods, and influencing factors. Constr Build Mater 2021;299:124279.
[5] Guo M, Tan Y. Interaction between asphalt and mineral fillers and its correlation to mastics' viscoelasticity. Int J Pavement Eng 2021;22(1):1–10.
[6] Chen JS, Kuo PH, Lin PS, Huang CC, Lin KY. Experimental and theoretical characterization of the engineering behavior of bitumen mixed with mineral filler. Mater Struct 2008;41:1015–24.
[7] Wang H, Al-Qadi IL, Faheem AF, Bahia HU, Yang SH, Reinke GH. Effect of mineral filler characteristics on asphalt mastic and mixture rutting potential. Transp Res Rec 2011;2208(1):33–9.
[8] Muniandy R, Aburkaba E, Taha R. Effect of mineral filler type and particle size on the engineering properties of stone mastic asphalt pavements. J Eng Res [TJER] 2013;10(2):13–32.
[9] Xu P, Chen Z, Cai J, Pei J, Gao J, Zhang J, et al. The effect of retreated coal wastes as filler on the performance of asphalt mastics and mixtures. Constr Build Mater 2019;203:9–17.
[10] Zhang J, Liu S, Yao Z, Wu S, Jiang H, Liang M, et al. Environmental aspects and pavement properties of red mud waste as the replacement of mineral filler in asphalt mixture. Constr Build Mater 2018;180:605–13.
[11] Nanda S, Berruti F. Municipal solid waste management and landfilling technologies: a review. Environ Chem Lett 2021;19(2):1433–56.
[12] Xu X, Leng Z, Lan J, Wang W, Yu J, Bai Y, et al. Sustainable practice in pavement engineering through value-added collective recycling of waste plastic and waste tyre rubber. Engineering 2021;7(6):857–67.
[13] Shekdar AV. Sustainable solid waste management: an integrated approach for Asian countries. Waste Manag 2009;29(4):1438–48.
[14] Xu X, Luo Y, Sreeram A, Wu Q, Chen G, Cheng S, et al. Potential use of recycled concrete aggregate (RCA) for sustainable asphalt pavements of the future: a state-of-the-art review. J Clean Prod 2022;344:130893.
[15] Yang B, Li H, Zhang H, Sun L, Harvey J, Tian Y, et al. Environmental impact of solid waste filler in porous asphalt mixture. Constr Build Mater 2021;303:124447.
[16] Woszuk A, Bandura L, Franus W. Fly ash as low cost and environmentally friendly filler and its effect on the properties of mix asphalt. J Clean Prod 2019;235:493–502.
[17] Al-Hdabi A. Laboratory investigation on the properties of asphalt concrete mixture with Rice Husk Ash as filler. Constr Build Mater 2016;126:544–51.
[18] Zhang H, Li H, Abdelhady A, Xie N, Li W, Liu J, et al. Fine solid wastes as a resource-conserving filler and their influence on the performance of asphalt materials. J Clean Prod 2020;252:119929.
[19] Chen M, Lin J, Wu S. Potential of recycled fine aggregates powder as filler in asphalt mixture. Constr Build Mater 2011;25(10):3909–14.
[20] Chen Z, Leng Z, Jiao Y, Xu F, Lin J, Wang H, et al. Innovative use of industrially produced steel slag powders in asphalt mixture to replace mineral fillers. J Clean Prod 2022;344:131124.
[21] Tayibi H, Choura M, Lopez FA, Alguacil FJ, Lopez-Delgado A. Environmental impact and management of phosphogypsum. J Environ Manage 2009;90(8):2377–86.
[22] Murali G, Azab M. Recent research in utilization of phosphogypsum as building materials. J Mater Res Technol 2023;25:960–87.
[23] Cao J, Wang Z, Ma X, Yang X, Zhang X, Pan H, et al. Promoting coordinative development of phosphogypsum resources reuse through a novel integrated approach: a case study from China. J Clean Prod 2022;374:134078.
[24] Meng X, Ding N, Lu B, Yang J. Integrated evaluation of the performance of phosphogypsum recycling technologies in China. Waste Manag 2023;171:599–609.
[25] Bilal E, Bellefqih H, Bourgier V, Mazouz H, Dumitraş D-G, Bard F, et al. Phosphogypsum circular economy considerations: a critical review from more than 65 storage sites worldwide. J Clean Prod 2023;414:137561.
[26] Wu F, Ren Y, Qu G, Liu S, Chen B, Liu X, et al. Utilization path of bulk industrial solid waste: a review on the multi-directional resource utilization path of phosphogypsum. J Environ Manage 2022;313:114957.
[27] Cuadri A, Navarro F, García-Morales M, Bolívar J. Valorization of phosphogypsum waste as asphaltic bitumen modifier. J Hazard Mater 2014;279:11–6.
[28] Amrani M, Taha Y, Kchikach A, Benzaazoua M, Hakkou R. Phosphogypsum recycling: New horizons for a more sustainable road material application. J Build Eng 2020;30:101267.
[29] Mehta S, Pastariya S, Bhargava A, Verma G, Bharadwaj A. Bitumen concrete mix design using cement and phosphogypsum as filler materials. Int J Adv Eng Res Sci 2020;7(6):296–300.
[30] Chattopadhyay DK, Raju K. Structural engineering of polyurethane coatings for high performance applications. Prog Polym Sci 2007;32(3):352–418.
[31] Huang T, Chen J, Li M, Tang Y, Lv S, Yu H, et al. Investigation on three-dimensional failure criterion of asphalt mixture considering the effect of stiffness. Constr Build Mater 2021;285:122431.
[32] Zhou X, Lu D, Du X, Wang G, Meng F. A 3D non-orthogonal plastic damage model for concrete. Comput Methods Appl Mech Eng 2020;360:112716.
[33] Lu D, Meng F, Zhou X, Zhuo Y, Gao Z, Du X. A dynamic elastoplastic model of concrete based on a modeling method with environmental factors as constitutive variables. J Eng Mech 2023;149(12):04023102.
[34] Das PK, Tasdemir Y, Birgisson B. Low temperature cracking performance of WMA with the use of the Superpave indirect tensile test. Constr Build Mater 2012;30:643–9.
[35] Li Z, Yang F, Yuan J, Cong L, Yu M. Study on preparation and pavement performance of polyurethane modified asphalt based on in-situ synthesis method. Constr Build Mater 2021;309:125196.
[36] Xia L, Cao D, Zhang H, Guo Y. Study on the classical and rheological properties of castor oil-polyurethane pre polymer (C-PU) modified asphalt. Constr Build Mater 2016;112:949–55.
[37] Cuadri A, García-Morales M, Navarro F, Partal P. Effect of transesterification degree and post-treatment on the in-service performance of NCO-functionalized vegetable oil bituminous products. Chem Eng Sci 2014;111:126–34.
[38] Navarro F, Partal P, García-Morales M, Martinez-Boza F, Gallegos C. Bitumen modification with a low-molecular-weight reactive isocyanate-terminated polymer. Fuel 2007;86(15):2291–9.
[39] Jiang W, Zhang M, Ren P, Xing C, Yuan D, Wu W. Development of porous asphalt mixture based on the synthesis of PTEMG and MDI polyurethane asphalt. Constr Build Mater 2024;411:134537.
[40] Li X, Li J, Wang J, Yuan J, Jiang F, Yu X, et al. Recent applications and developments of Polyurethane materials in pavement engineering. Constr Build Mater 2021;304:124639.
[41] Izquierdo M, García-Morales M, Martínez-Boza F, Navarro F. Thermo-mechanical properties and microstructural considerations of MDI isocyanate-based bituminous foams. Mater Chem Phys 2014;146(3):261–8.
[42] Li T, Guo Z, Liang D, Luo S, Zhang Y, Hong B, et al. Chemical and physical effects of polyurethane-precursor-based reactive modifier on the low-temperature performance of bitumen. Constr Build Mater 2022;328:127055.
[43] Lu D, Liang J, Du X, Ma C, Gao Z. Fractional elastoplastic constitutive model for soils based on a novel 3D fractional plastic flow rule. Comput Geotech 2019;105:277–90.
[44] Ou L, Li R, Zhu H, Zhao H, Chen R. Upcycling waste phosphogypsum as an alternative filler for asphalt pavement. J Clean Prod 2023;420:138332.
[45] Zhang L, Zhang A, Li K, Wang Q, Han Y, Yao B, et al. Research on the pretreatment and mechanical performance of undisturbed phosphogypsum. Case Stud Constr Mater 2020;13:e00400.
[46] Gong X, Liu Q, Chen P, Wang H, Liu X, Chen S, et al. Modification mechanism of green polyurethane modified asphalt prepared by in-situ polymerization. Constr Build Mater 2024;448:138243.
[47] Izquierdo M, Navarro F, Martínez-Boza FJ, Gallegos C. Novel stable MDI isocyanate-based bituminous foams. Fuel 2011;90(2):681–8.
[48] Li T, Carreño Gómez NH, Lu G, Liang D, Wang D, Oeser M. Use of polyurethane precursor–based modifier as an eco-friendly approach to improve performance of asphalt. J Trans Eng, Part B: Pavements 2021;147(3):04021031.
[49] Huang G, Yang T, He Z, Yu L, Xiao H. Polyurethane as a modifier for road asphalt: a literature review. Constr Build Mater 2022;356:129058.
[50] Ting JH, Khare E, DeBellis A, Orr B, Jourdan JS, Martín-Martínez FJ, et al. Role of methylene diphenyl diisocyanate (MDI) additives on SBS-modified asphalt with

improved thermal stability and mechanical performance. Energy Fuel 2021;35(21):17629–41.
[51] Carrera V, Partal P, García-Morales Ms, Gallegos Cs, Páez A. Influence of bitumen colloidal nature on the design of isocyanate-based bituminous products with enhanced rheological properties. Ind Eng Chem Res 2009;48(18):8464–70. https://doi.org/10.1021/ie9004404.
[52] Carrera V, Cuadri A, García-Morales M, Partal P. Influence of the prepolymer molecular weight and free isocyanate content on the rheology of polyurethane modified bitumens. Eur Polym J 2014;57:151–9.
[53] Cuadri A, García-Morales M, Navarro F, Partal P. Isocyanate-functionalized castor oil as a novel bitumen modifier. Chem Eng Sci 2013;97:320–7.
[54] Peng Y, Zhao T, Miao J, Kong L, Li Z, Liu M, et al. Evaluation framework for bitumen-aggregate interfacial adhesion incorporating pull-off test and fluorescence tracing method. Constr Build Mater 2024;451:138773.